05

Precession Dynamics of the Uniaxial Nanoparticle Magnetization in the Ferromagnetic Resonance Region

© A.M. Shutyi [1], T.M. Vasilevskaya [2], D.I. Sementsov [1,¶], S.V. Eliseeva [1]

[1] Ulyanovsk State University,
Ulyanovsk, Russia
[2] Ulyanovsk Civil Aviation Institute,
Ulyanovsk, Russia

¶ E-mail: sementsovdi42@mail.ru

The influence of the shape parameter (oblateness) of a uniaxial ellipsoidal nanoparticle on the dynamics of its magnetic moment upon magnetization along the symmetry axis and excitation by a weak transverse high-frequency field in the region of parameters where the equilibrium magnetic moment of the nanoparticle and the external static field is noncollinear has been studied. It is shown that as the oblateness increases, the irregularity of the oscillations increases, which at first affects only their amplitude, but then also the time dependence. The intervals of the shape parameter (or frequency), where various nonlinear modes of precession are realized — dynamic bistability, complex spatial attractors and chaos, were revealed using bifurcation diagrams.

Keywords: ellipsoidal nanoparticle, „easy" axis, effective anisotropy, ferromagnetic resonance, high frequency field, bistability, regular and chaotic precession.

1. Introduction

Detection and analysis of magnetic nanoparticle (NP) and regular lattice response to persistent, high frequency and pulsed external fields have been of great interest among researchers over the last years. Applicability of digital data storage media is based on the modification of equilibrium magnetic moment configuration of an individual NP or group of NP exposed to a magnetic field pulse. For this, information can be read by exciting the resulting configuration by a weak radio pulse at the ferromagnetic resonance (FMR) frequency [1–6].

Magnetic NP assemblies are also increasingly coming into use in various biomedicine areas. In particular, they are used to manufacture contrasting agents for magnetic resonance imaging, biomolecule and microbiological object sensors, and targetable drug carriers [7]. One of such important areas includes control of tumors in a living body using magnetic hyperthermia methods [8–10]. NP exited by a low-frequency magnetic field and injected into a tumor area warm up this area locally in a controlled manner resulting in disruption of tumor cells. For effective warm-up process, NP shall respond to the external magnetic field with the appropriate frequency and amplitude absorbing and transferring the magnetic field energy in the form of heat to the surrounding tissues. Ferrite — Fe_3O_4 — is the best-investigated material for hyperthermia due to high biological compatibility and satisfactory magnetic properties. High Curie temperature (550°C) is a disadvantage of this material due to which NP may be heated up to 100°C and

higher depending on the frequency, applied magnetic field amplitude and exposure time. Such high temperatures are harmful for normal tissues. Therefore, the research efforts are focused on achievement of magnetic materials whose Curie temperature is within 45°C. When such temperatures are reached, NP go into their paramagnetic state and the heating process is terminated automatically [11].

Dynamic behavior of an individual single-domain NP depends significantly on its size and symmetry, equilibrium magnetization state, type and magnitude of magnetic anisotropy. Many studies in this field are focused on investigations of FMR in elliptical NP or in nanometer-thick rectangular microstrips with uniaxial or cubic magnetic anisotropy, which are regarded as one of the main geometric elements for data recording and processing. For this, behavior may be controlled by an external alternating field of various polarization and time dependence [6,12–16].

At this point, dynamic bistability states and various nonlinear conditions (quasiregular behavior, stochastic vibrations, random response) have been detected in above systems, with each condition having its specific features manifesting themselves in high-frequency precession magnetic moment dynamics of an individual NP [17–24].

In [25], equilibrium states were obtained for a magnetically uniaxial NP with the „easy" axis and bias field orientation along the axis of symmetry and with various values of the particle „flatness". Numerical solution of the Landau–Lifshitz–Helmholtz (LLH) equation is used to examine the aspects of resonance behavior when a high-frequency low-amplitude field is activated for a region with

collinear magnetic moment and static field. For a weakly flattened NP, a frequency range has been detected where FMR deviation for linear resonance and a nutation type of resonance precession are observed and dynamic bistability is implemented.

This study investigates the aspects of precession behavior associated with NP shape modification for a parameter region where the equilibrium magnetic moment state of NP does not coincide any longer with the external static field direction. Magnetic moment precession in this range is usually nonlinear, dynamic bistability, complex spatial attractors and chaos take place.

2. Equilibrium states

Consider a single-domain NP with a spheroid shape. In case of uniform magnetization, demagnetization field energy density may be written as $F_r = 0.5(\mathbf{M}\hat{N}\mathbf{M})$, where $\mathbf{M}$ is the NP magnetization, and $\hat{N}$ is a diagonal tensor of demagnetization coefficients [26,27]. Components of this tensor are associated with $N_x + N_y + N_z = 4\pi$ and depend on a shape parameter longitudinal and transverse spheroid semiaxes ratio $n = l_{\parallel}/l_{\perp}$. For the spheroid, it is convenient to introduce $N_{\perp} = N_x = N_y$, $N_{\parallel} = N_z$ and $\Delta N = N_{\perp} - N_{\parallel}$, where ΔN for elongated and flattened spheroids is defined by the following expressions

$$\frac{\Delta N}{2\pi} = 1 - \frac{3}{n^2 - 1}$$
$$\times \left[\frac{n}{\sqrt{n^2 - 1}} \ln\left(n + \sqrt{n^2 - 1}\right) - 1 \right] > 0, \quad n > 1,$$

$$\frac{\Delta N}{2\pi} = 1 - \frac{3}{n^2 - 1}$$
$$\times \left[\frac{n}{\sqrt{n^2 - 1}} \arcsin\sqrt{n^2 - 1} - 1 \right] < 0, \quad n < 1, \quad (1)$$

NP will be assumed to have uniaxial anisotropy whose „easy" axis coincides with the symmetry axis of the sample. In this case, magnetic anisotropy energy density $F_u = -(K_u/M^2)(\mathbf{Mn})^2$, where K_u is the uniaxial anisotropy constant, $\mathbf{n}$ is the unit vector of the „easy" axis. In the presence of external static field H oriented along the symmetry axis of NP, dependence of the magnetic NP energy on angle θ is written as

$$F(\theta) = -MH\cos\theta - \left(K_u - \frac{1}{2}N_{\parallel}M^2\right)\cos^2\theta$$
$$+ \frac{1}{2}N_{\perp}M^2\sin^2\theta, \quad (2)$$

where $N_{\parallel} = (4\pi - 2\Delta N)/3$, $N_{\perp} = (4\pi + \Delta N)/3$.

Equilibrium values of polar angle θ_0 defining the directions of vector $\mathbf{M}_0$ with respect to the symmetry axis of the spheroid (axis OZ) are found from $\partial F/\partial\theta = 0$. Taking into
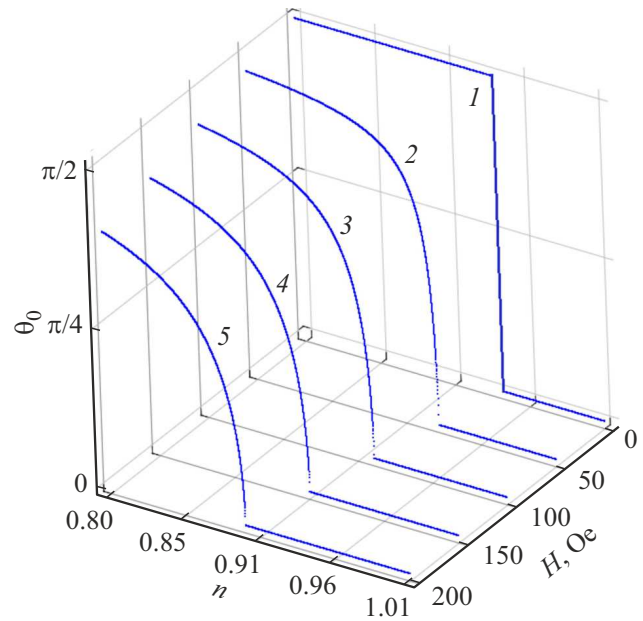

Figure 1. Dependences of the equilibrium polar angle of vector $\mathbf{M}_0$ on shape parameter n at $H = (0, 50, 100, 150, 200)$ Oe (curves *1−5*).

account (2), the equilibrium condition is written as

$$\sin\theta_0\left[H + (H_u + M_0\Delta N)\cos\theta_0\right] = 0, \quad (3)$$

where $H_u = 2K_u/M_0$ is the uniaxial anisotropy field Taking into account the „easy" axis orientation along the symmetry axis of the sample, it is convenient to inject effective anisotropy field $H_{KN} = H_u + M_0\Delta N$, which defines to a great extent NP magnetization behavior. It follows from (3) that for elongated and spherical NP (i.e. $n \geq 1$), equilibrium polar angle $\theta_0 = 0$ at any field value H. zero value of θ_0 is maintained also for a flattened NP $n < 1$) until $\Delta N = -(H + H_u)/M_0$ is reached. With further decrease in the shape parameter, θ_0 varies in accordance with the expression

$$\cos\theta_0 = -H(H_u + \Delta N M_0)^{-1}. \quad (4)$$

Figure 1 shows the dependence of equilibrium polar angle θ_0 on shape parameter n obtained for constitutive parameters $K_u = 10^5$ erg/cm^4 and $4\pi M_0 = 10^4$ Gs (NP parameters close to 80Ni20Fe permalloy characteristics) and external static field $H = (0, 50, 100, 150, 200)$ Oe (curves *1−5*). It can be seen that vector $\mathbf{M}_0$ in the equilibrium state at the given values of the external field remains parallel to the external field and NP symmetry axis $\theta_0 = 0$ only at $\mathbf{n} \geq 0.94$, 0.928, 0.917, 0.906, 0.895 (curves *1−5*). At lower values of the shape parameter, θ_0 starts growing dramatically tending to a value near $\pi/2$.

Variation of NP shape parameter n results in considerable modification of H_{KN} and ΔN (Figure 2). It can be seen that the effective anisotropy field and ΔN depending on n have both negative and positive value regions. In this case, field

$H_{KN} \simeq 0$ with $n \simeq 0.94$, and $\Delta N = 0$ with $n = 1$. Variation of n near the given values results in sign change of H_{KN} and ΔN.

3. Main precession behavior equations

Dependence of **M** orientation on time and, therefore, its precession behavior for various cases of biasing with static field **H** with high-frequency pumping by alternating field **h** are described by the LLH equation [26,27]:

$$\frac{\partial \mathbf{M}}{\partial t} = -\gamma \mathbf{M} \times \mathbf{H}^{ef} + \frac{\alpha}{M} \mathbf{M} \times \frac{\partial \mathbf{M}}{\partial t}, \qquad (5)$$

where $\gamma = 1.76 \cdot 10^7 \, (\text{Oe} \cdot \text{s})^{-1}$, α is a dimensionless attenuation constant, effective magnetic field.

$$\mathbf{H}^{eff} = \mathbf{H} + \mathbf{h}(t) + \frac{2K_u}{M_0} \mathbf{n} + \hat{N}\mathbf{M}. \qquad (6)$$

The frequency of resonance magnetization precession (with $h \ll H$) is generally determined by expression

$$\omega_{res} = \frac{\gamma}{M_0 \sin \theta_0} \left[\left(\frac{\partial^2 F}{\partial \varphi^2} \right)_0 \left(\frac{\partial^2 F}{\partial \theta^2} \right)_0 - \left(\frac{\partial^2 F}{\partial \varphi \partial \theta} \right)_0^2 \right]^{1/2}, \qquad (7)$$

where the second derivatives of free energy are calculated for the equilibrium values of φ_0 and θ_0. For magnetic biasing of NP along the symmetry axis ($\mathbf{H} \parallel \mathbf{n} \parallel OZ$) in the basal plane, there is no dependence on azimuthal angle φ, and equilibrium angle φ_0 (counted, for example, from axis OX) can be taken equal to zero. In this case, in the region of values of n where the equilibrium angle θ_0 is equal to zero, dependence of the resonance frequency on the external field taking into account (2) and (7) is determined by the following expression

$$\omega_{res} = \gamma \left(H + \frac{2K_u}{M_0} + M_0 \Delta N \right) = \gamma (H + H_{KN}). \qquad (8)$$

Figure 2 shows that even rather small deviation of NP shape from nonsphericity significantly affects K_{KN} and resonance dependences in general. It will be shown below that shape parameter n also affects the precession magnetic moment behavior of an ellipsoidal NP.

Consider the NP magnetization behavior under the impact to transverse magnetic field $\mathbf{h}(t) = \mathbf{h}_0 \sin \omega t$ with low amplitude ($h_0 \ll H$) and transverse orientation ($\mathbf{h}_0 \perp \mathbf{H}$), hereinafter field $\mathbf{h}(t)$ will be assumed as polarized along axis OY). Numerical solution of the LLH equations was carried out by the Runge–Kutta method. Statistic field was chosen close to the resonance value for NP with the constitutive parameters listed above at the specified biasing conditions.

Figure 2 shows that there are two parameter regions, in one of which vectors $\mathbf{M}_0$ and $\mathbf{H}$ are noncollinear, and collinear in the other region. Precession behavior in the collinearity region was reviewed in detail in [25]. The main aspects of the NP magnetic moment behavior during
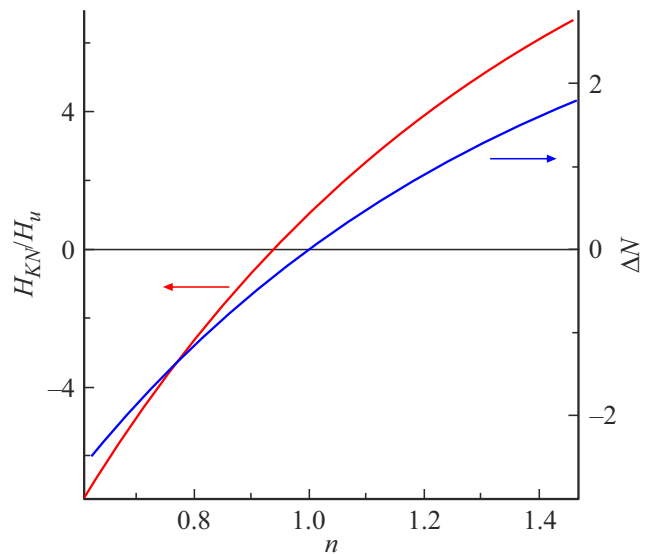

Figure 2. Dependence of effective anisotropy field H_{KN} and ΔN on the ellipsoidal NP semiaxes ratio.

transverse pumping with a weak high-frequency field are summarized below. With n, for which effective anisotropy field $H_{KN} > 0$, relatively low amplitudes of the steady-state circular precession paths ($M_x, M_y \ll M_0$) occur in plane (M_x, M_y). For n, when $H_{KN} < 0$, precession paths incur more apparent elliptical distortions with decreasing n. In these conditions, a nonlinear effect starts manifesting itself and involves imposition of double frequency nutation motion on the circular precession with microwave field frequency, as a result the path becomes elliptical. Attention is also paid to the fact that, with decreasing n, the precession amplitude increases and at n, to which $H_{KN} \simeq 0$ corresponds, the amplitude reaches $M_x \simeq M_0/2$.

4. Dynamics with noncollinearity of vectors $\mathbf{M}_0$ and $\mathbf{H}$

Let us now consider the magnetization behavior of an NP whose equilibrium magnetic moment orientation does not coincide with the symmetry axis OZ, i.e. polar angle $\theta \neq 0$ is equilibrium. This region in Figure 1 corresponds to a non-linear dependence of $\theta_0(n)$. During precession motion under the impact of the alternating field linearly polarized along the axis Y, the path of vector $\mathbf{M}(t)$ differ considerably from closed circular or weakly elliptical paths appearing in case of $\mathbf{M}_0 \parallel \mathbf{H}$. Figure 3 shows projections of spatial paths of vector $\mathbf{M}(t)$ on plane XY during precession motion under the impact of an alternation field linearly polarized along the axis Y at $H = 150 \, \text{Oe}$, $n = 0.9$, 0.89, 0.88, 0.87, 0.85 (curves *1−5*), microwave field amplitude $h_0 = 0.1 \, \text{Oe}$ and frequency $\omega = (1, 1.05) \cdot 10^8 \, \text{s}^{-1}$ (curves *1−3, 5; 4*). It can be seen that with increasing flatness of NP (i.e. decreasing n), the arc covered by the precession behavior increases and develops into a circle at $n = 0.85$. Precession amplitude considerably depends on the alternating field parameters.

Figure 4 shows the dependence of z-component of magnetization on time for the cases satisfying those shown in Figure 3. It can be seen that vibrations with a small
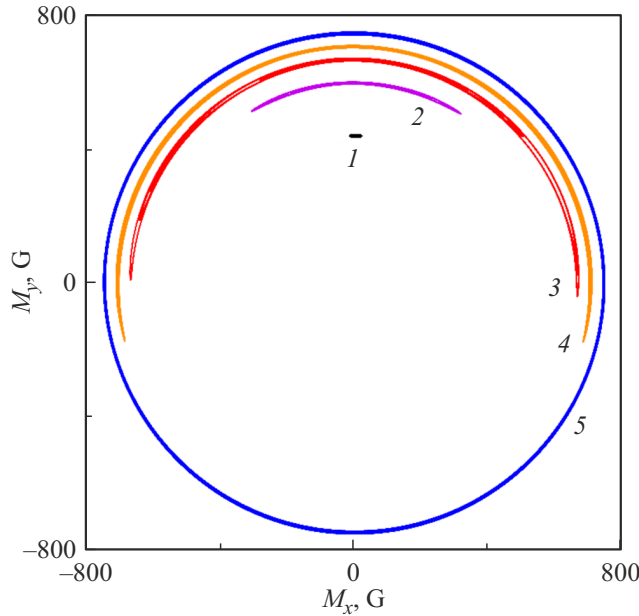

Figure 3. NP magnetization projection on plane XY with $n = 0.9$, 0.89, 0.88, 0.87, 0.85 (curves $1-5$) and $\omega = (1, 1.05) \cdot 10^8 \, \text{s}^{-1}$ (curves $1-3, 5; 4$), $H = 150 \, \text{Oe}$, $h_0 = 0.1 \, \text{Oe}$.
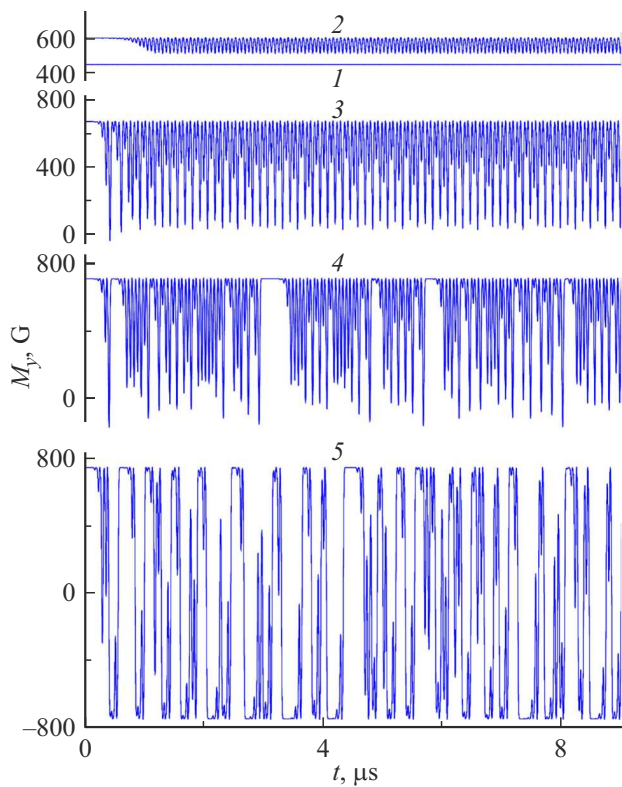

Figure 4. Dependence of M_y component on time at $H = 150 \, \text{Oe}$, $h_0 = 0.1 \, \text{Oe}$, $n = 0.9$, 0.89, 0.88, 0.87, 0.85 (curves $1-5$), (curves $1-3, 5; 4$).
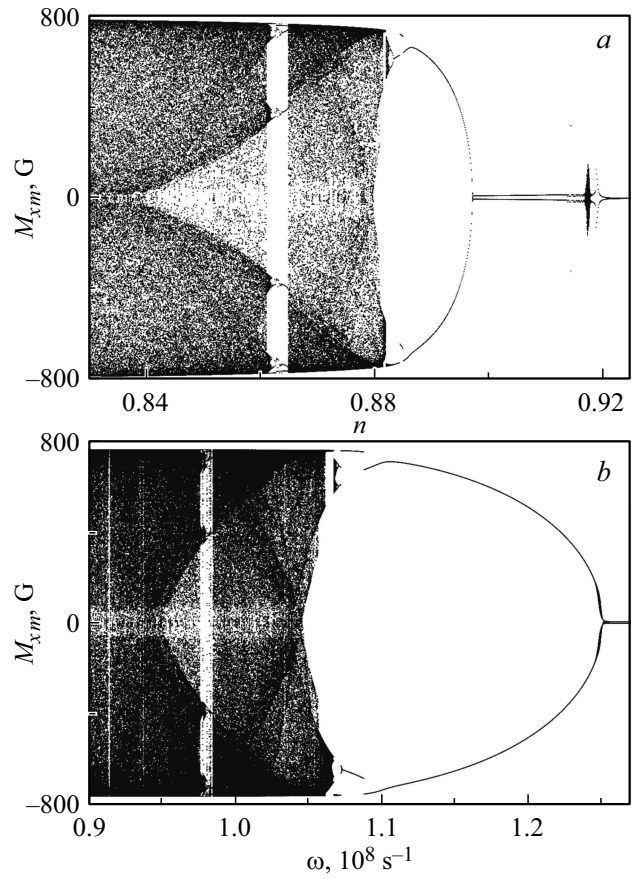
Figure 5. Dependences of extreme component M_{xm} on n at $\omega = 1 \cdot 10^8 \, \text{s}^{-1}$ (a) and on frequency at $n = 0.87$ (b), $h_0 = 0.1 \, \text{Oe}$, $H = 100 \, \text{Oe}$.

precession arc are close to harmonic vibrations. Irregularity of vibrations increases with decreasing n and increasing precession arc and at first affects their amplitude only, but then also affects the time dependence. Precession irregularity becomes more pronounced for a circular path projection (curve 5 in Figure 3 and 4).

For more complete analysis of the influence of NP flatness on magnetization behavior, bifurcation diagrams (Figure 5) will be plotted, i.e. dependences of the extreme value of one of components of magnetization **M** (here, components $M_{xm} \equiv M_{x\,\text{max}}, M_{x\,\text{min}}$) on n with $\omega = 10^8 \, \text{s}^{-1}$ (a) and on the alternating field frequency with $n = 0.87$ (b) with $h_0 = 0.1 \, \text{Oe}$ and $H = 100 \, \text{Oe}$. In the absence of magnetization precession, the variable value (n or ω) corresponds to only one point ($M_{x\,\text{max}} = M_{x\,\text{min}}$) on the diagram; in case of regular vibrations — two or a denumerable number of points; if the parameter value on the diagram corresponds to a nondenumerable number of points (which merge into dark regions when the numerical simulation time increases), a chaotic (quasiregular in some cases) dynamic mode occurs. Diagram (a) shows that precession is almost absent in case of sufficiently small flatness ($0.92 < n < 1$), since the effective magnetic field
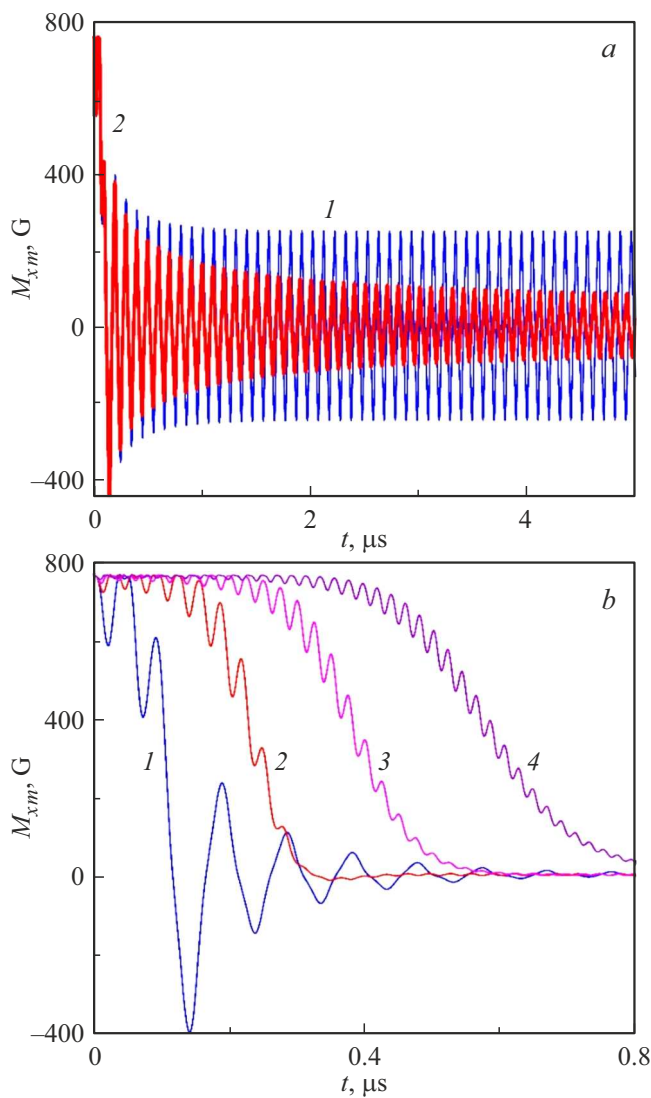
Figure 6. Dependences of component M_x on time during NP remagnetization under the impact of alternating field $h_y(t)$ at $\omega = (1.24, 1.25) \cdot 10^8 \, \text{s}^{-1}$ (curves $1-4$, a) and $\omega = (1.3, 2, 2.5, 3) \cdot 10^8 \, \text{s}^{-1}$ (curves $1-4$, b), $n = 0.87$, $h_0 = 0.1 \, \text{Oe}$, $H = 100 \, \text{Oe}$.

which keeps magnetization near the equilibrium position is still strong. In case of $0.897 < n < 0.92$, low-amplitude vibrations ($|M_{xm}| \approx 10 \, \text{G}$) occur. Further decrease of n results in quickly rising amplitude of the regular precession behavior of magnetization up to $|M_{xm}| \approx 650 \, \text{G}$.

Then the vibration trajectory becomes more complicated, and at $n < 0.882$ the behavior enters the region of chaotic vibrations where narrow regular precession regions exist with complex trajectories and a period being a multiple of the alternating field period. Diagram (b) is identical: precession is almost absent at alternating field frequency $\omega \geq 1.25 \cdot 10^8 \, \text{s}^{-1}$ (i.e. the said parameters are rather far from the resonance values), the amplitude of regular vibrations increases up to $|M_{xm}| \approx 750 \, \text{G}$ with decreasing frequency, the magnetization behavior at $\omega \leq 1.07 \cdot 10^8 \, \text{s}^{-1}$

is in the chaos region, including narrow regions the regular precession. The structure of the given diagrams also shows that the random mode attractors will change with modification of the given parameters.

Figure 6, a, b is supported by the time dependence of component M_x for NP with $n = 0.87$ in static field $H = 100 \, \text{Oe}$ when alternating field $h_y(t)$ is enabled with $h_0 = 0.1 \, \text{Oe}$ and $\omega = (1.3, 2, 2.5, 3) \cdot 10^8 \, \text{s}^{-1}$ (curves $1-4$; a) and (curves $1, 2$; b). In the initial state, $M_y(0) = 0$ and the polar angle corresponds to the equilibrium value for the given n and H. It can be seen that all frequencies in case (a) are in the region which corresponds to the absence of vibration mode (see the bifurcation diagram). Therefore, upon activation of a high-frequency field, the NP magnetic moment in the quickly decaying vibration mode comes to rest within a relatively short time ($\tau < 1 \, \mu\text{s}$). In case (b), the frequency for curve 1 is already in the high-amplitude vibrations region, therefore, magnetization under the action of an alternating field goes from the initial state to a steady-state vibration mode with an amplitude considerably different from zero. For curve 2, the frequency lies almost on the interface between the vibrations region and the region without vibrations. Therefore, vibrations generated by the alternating field are decaying vibrations with a long decay time ($\tau \gg 1 \, \mu\text{s}$).

Now, consider the main regular and random precession modes for NP with $n = 0.87$, that are established at various alternating field frequencies with $h_0 = 0.1 \, \text{Oe}$ and $H = 100 \, \text{Oe}$.

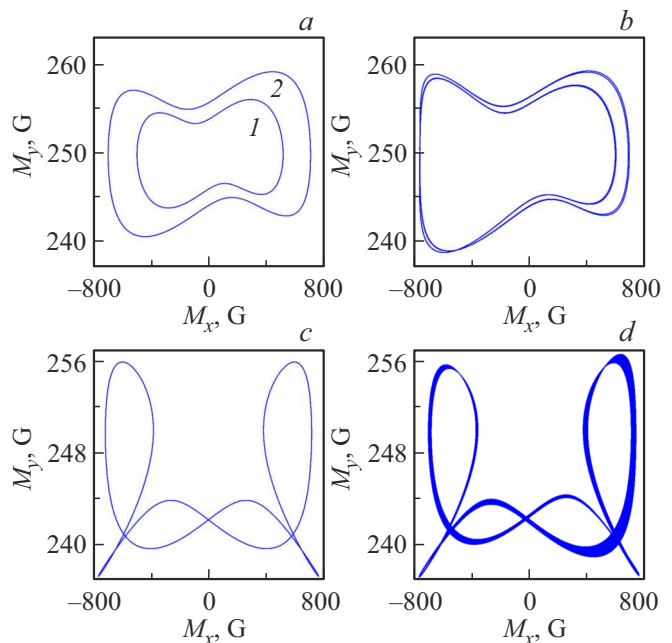Figure 7 shows the projections of **M** paths on the XY plane in case of regular behavior

Figure 7. Projections of **M** paths in case of regular behavior with $\omega = (1.2, 1.12) \cdot 10^8 \, \text{s}^{-1}$ (a — curves $1, 2$) and $\omega = (1.07, 0.98) \cdot 10^8 \, \text{s}^{-1}$ (b, c); in case of low randomness with $\omega = 0.977 \cdot 10^8 \, \text{s}^{-1}$ (d); $h_0 = 0.1 \, \text{Oe}$, $H = 100 \, \text{Oe}$, $n = 0.87$.
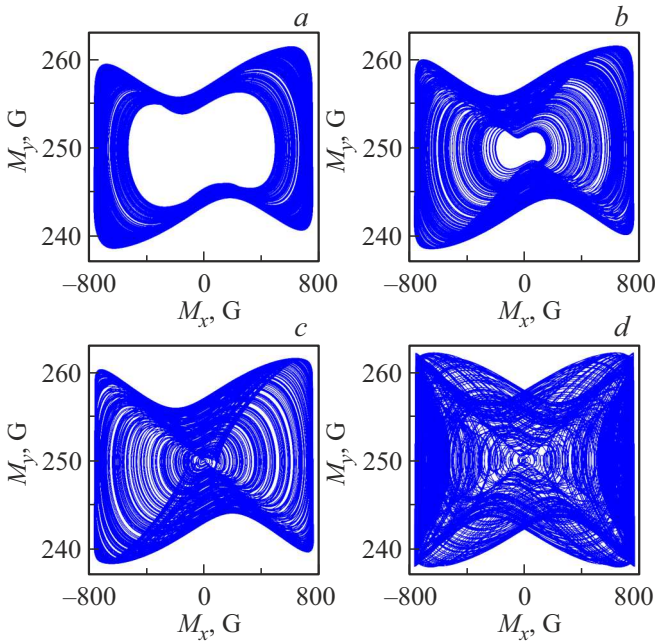
Figure 8. Projections of **M** paths in case of random behavior with $\omega = (1.06, 1.05, 1.04, 1) \cdot 10^8 \, \text{s}^{-1}$ $(a{-}d)$; $h_0 = 0.1 \, \text{Oe}$, $H = 100 \, \text{Oe}$, $n = 0.87$.

at $\omega = (1.2, 1.12) \cdot 10^8 \, \text{s}^{-1}$ $(a$ — curves *1, 2)*, $\omega = (1.07, 0.98) \cdot 10^8 \, \text{s}^{-1}$ (b, c) and in case of low randomness at $\omega = 0.977 \cdot 10^8 \, \text{s}^{-1}$ (d). It should be noted that the attractor (d) occurs due to randomization and expansion of the regular mode attractor (c). This mode is included in the narrow regular behavior region within the chaos region (see the bifurcation diagram), and randomization of vibrations grows dramatically with further frequency decrease. Modes (a) have the simplest attractors and are established at relatively high frequencies, up to frequencies at which precession stops.

Regular precession (b) period is a multiple of the alternating field period $T = 4 \cdot 2\pi/\omega$. Projections of the attractors on the XY plane is a circle in cases (c, d) and an arc in cases (a, b). Figure 8 shows the projections of **M** on the XZ plane for the above-mentioned field and NP flatness parameters and $\omega = (1.06, 1.05, 1.04, 1) \cdot 10^8 \, \text{s}^{-1}$ $(a{-}d)$; these projections show the development of randomization with a little decrease in the alternating field frequency. The maximum randomization takes place when circle (d) is a projection of attractors on the XY plane, and in cases $(a{-}c)$, these projections are of an arc type.

It should be noted that such manifestations of nonlinearity and random behavior shall be observed not only for ellipsoidal NP, but also for cylindrical NP. Moreover, internal field inhomogeneity in such NP shall expand (by $n = l/d$) the random behavior region. Therefore, analysis of the maximum thermal response conditions for particles having a cylindrical disc shape taking into account the random magnetization behavior is of interest and requires separate study (e.g. for hyperthermia applications).

5. Conclusion

The analysis shows that a set of features associated with NP shape (flatness) and nonlinearity manifestation is observed in the FMR spectrum of a single-domain spheroidal nanoparticle whose „easy" axis coincides with the symmetry axis during biasing along this axis and traditional transverse pumping by the weak alternating field $(h \ll H_0)$. In the parameter region where collinearity of the equilibrium magnetic moment of NP and external static field is implemented, these features primarily include large resonance precession angles, at which the amplitude is $0.5M_0$; elliptical disturbances of the steady-state precession path at a negative effective anisotropy field; presence of the frequency range where the dynamic bistability is implemented at $n \simeq 0.93$ and precession which becomes substantially nonlinear. In the NP equilibrium magnetic moment and external static field noncollinearity region, it is shown that vibration irregularity grows with increasing flatness, which initially affects only vibration amplitude, and then affects the time dependence; using bifurcation diagrams, shape (or frequency) ranges were identified where various nonlinear precession modes are implemented — dynamic bistability, complex spatial attractors and chaos.

It should be noted that, with the amplitude and frequency of the pumping field used herein, the uniform mode is very far from the spin-wave mode in terms of frequency, therefore, there is no energy transfer from the uniform precession to spin waves and no development of spin-wave instabilities [28].

Finally, restrictions imposed on the NP size due to the magnetization uniformity should be also noted:

— in the presence of a high-frequency field, maximum NP size d should be much smaller than spin layer thickness δ. For permalloy NP, $d \ll \delta \approx 10^{-4} \, \text{cm}$ shall be met;

— thermal fluctuations may have a considerable impact on the precession behavior of NP magnetization. Their influence is described by multiplier $\exp(-\Delta U/k_B T)$ [3], where ΔU is a potential barrier separating an the „easy" and „hard" directions. Thermal excitation does not disturb the precession behavior, if NP size $d > d_{\min} \approx 10 \, \text{nm}$;

— NP single domain requirement that can be met when NP radius is smaller than $R_{cr} \approx \sigma_s/M_0^2$, where domain boundary surface energy (for permalloy) $\sigma_s \approx 1 \, \text{erg/cm}^2$. Therefore, for the NP of interest, $d < 2R_{cr} \approx 30 \, \text{nm}$ is required. Thus, $d \in (10{-}30) \, \text{nm}$ is the best NP size for observation of the effects described herein. However, it should be noted that according to [29] metallic particles with $d \approx 40{-}50 \, \text{nm}$ shall be considered as single-domain.

Conflict of interest

The authors declare that they have no conflict of interest.

A.M. Shutyi, *T.M. Vasilevskaya, D.I. Sementsov, S.V. Eliseeva*

References

[1] E.Z. Meilikhov, R.M. Farzetdinova. JMMM **268**, 237 (2004).

[2] N. Eibagi, J.J. Kan, F.E. Spada, E.E. Fullerton. IEEE Magn. Lett. **3**, 4500204 (2012).

[3] E.Z. Meilikhov, R.M. Farzetdinova. FTT **56**, 2326 (2014). (in Russian).

[4] R. Berger, J.-C. Bissey, J. Kliava, H. Daubric, C. Estournéset. JMMM **234**, 535 (2001).

[5] V. Flovik, F. Macia, J.M. Hernandez, R. Bručas, M. Hanson, E. Wahlström. Phys. Rev. B **92**, 104406 (2015).

[6] R.B. Gorev, E.V. Skorokhodov, V.L. Mironov. FTT **58**, *11*, 2135 (2016). (in Russian).

[7] Yu.A. Koksharov, S.P. Gubin, I.V. Taranov, G.B. Khomutov, Yu.V. Gulyaev. RE **67**, *2*, 99 (2022). (in Russian).

[8] S. Dutz, R. Hergt. Nanotechnology **25**, *45*, 452001 (2014).

[9] E.A. Périgo, G. Hemery, O. Sandre, D. Ortega, E. Garaio, F. Plazaola, F. Teran. Applied Physics Reviews **2**, *4*, 041302 (2015).

[10] N.A. Usov, M.S. Nesmeyanov, E.M. Gubanova, N.B. Epshtein. Beilstein J. Nanotechnol. **10**, *1*, 305 (2019).

[11] A.S. Kamzin. FTT **59**, *1*, 149 (2017). (in Russian).

[12] G. Gubbiotti, G. Carlotty, T. Okuno, L. Giovannini, F. Montoncello, F. Nizzoli. Phys. Rev. B **72**, 184419 (2005).

[13] K.D. Usadel. Phys. Rev. B **73**, 212905 (2006).

[14] Z. Zhao, N. Garraud, D.P. Arnold, C. Rinaldi. Phys. Med. Biol. **65**, *2*, 025014 (2020).

[15] J. Rácz, P.F. De Chatel, I.A. Szabó, L. Szunyogh, I. Nándori. Phys. Rev. E **93**, *1*, 012607 (2016).

[16] T.M. Vasilevskaya, D.I. Sementsov, A.M. Shutyi. FTT **64**, *2*, 200 (2022). (in Russian).

[17] A.M. Ferona, R.E. Camley. Phys. Rev. B **95**, *10*, 104421 (2017).

[18] D.V. Vagin, O.P. Polyakov. JMMM **320**, *24*, 3394 (2008).

[19] D. Laroze, P. Vargas, C. Cortes, G. Gutierrez. JMMM **320**, *8*, 1440 (2008).

[20] R.K. Smith, M. Grabowski, R.E. Camley. JMMM **321**, *20*, 3472 (2009).

[21] R.K. Smith, M. Grabowski, R.E. Camley. JMMM **322**, *15*, 2127 (2010).

[22] M.G. Phelps, K.L. Livesey, A.M. Ferona, R.E. Camley. Europhys. Lett. **109**, *3*, 37007 (2015).

[23] A.M. Shutyi, S.V. Eliseeva, D.I. Sementsov. Phys. Rev. B **91**, *2*, 024421 (2015).

[24] A.M. Shutyi, D.I. Sementsov. JMMM **401**, 1033 (2016).

[25] A.A.M. Shutyi, T.M. Vasilevskaya, D.I. Sementsov. FTT **64**, *6*, 646 (2022). (in Russian).

[26] A.G. Gurevich, G.A. Melkov. Magnitnye kolebaniya i volny. Nauka, M. (1994).

[27] V.G. Shavrov, V.I. Shcheglov. Magnetization dynamics in conditions of its orientation change. Fizmatlit, M. (2019). (in Russian).

[28] P.E. Zilberman, A.G. Temiryazev, M.P. Tikhomirova. ZhETF, **108**, 281 (1995). (in Russian).

[29] S.A. Nepiyko. Fizicheskiye svoistva malykh metallicheskikh chastits. Nauk. dumka, Kiev (1985). (in Russian).

Translated by E.Ilyinskaya